# Simulation of Solution Phase Electron Transfer in a Compact Donor−Acceptor Dyad

Tim Kowalczyk, Lee-Ping Wang, and Troy Van Voorhis*

Department of Chemistry, Massachusetts Institute of Technology, Cambridge, Massachusetts 02139, United States

S *Supporting Information*

ABSTRACT: Charge separation (CS) and charge recombination (CR) rates in photosynthetic architectures are difficult to control, yet their ratio can make or break photon-to-current conversion efficiencies. A rational design approach to the enhancement of CS over CR requires a mechanistic understanding of the underlying electron-transfer (ET) process, including the role of the environment. Toward this goal, we introduce a QM/MM protocol for ET simulations and use it to characterize CR in the formanilide−anthraquinone dyad (FAAQ). Our simulations predict fast recombination of the charge-transfer excited state, in agreement with recent experiments. The computed electronic couplings show an electronic state dependence and are weaker in solution than in the gas phase. We explore the role of cis−trans isomerization on the CR kinetics, and we find strong correlation between the vertical energy gaps of the full simulations and a collective solvent polarization coordinate. Our approach relies on constrained density functional theory to obtain accurate diabatic electronic states on the fly for molecular dynamics simulations, while orientational and electronic polarization of the solvent is captured by a polarizable force field based on a Drude oscillator model. The method offers a unified approach to the characterization of driving forces, reorganization energies, electronic couplings, and nonlinear solvent effects in light-harvesting systems.
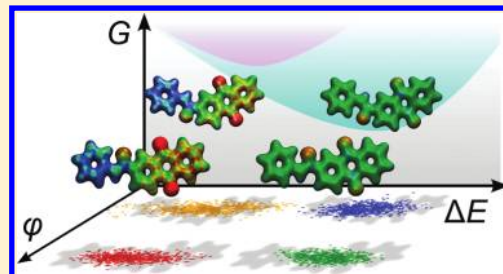
■ INTRODUCTION

Electron-transfer (ET) reactions are crucial steps in the storage of solar energy in chemical bonds. Whether in biological or bioinspired light-harvesting systems[1,2] or in advanced semiconductor materials,[3−5] the same three-step mechanism underlies the conversion of incident photon flux into photocurrent. Absorption of visible light by a photosensitive structure, such as a dye molecule or a semiconducting metal, generates a localized excited state. The availability of lower-energy electronic states with enhanced charge separation drives an ET process, resulting in an intermediate, charge-transfer (CT) excited state. The CT state can further separate into free charges, completing the photovoltaic process.

Synthetic light-harvesting systems have very high standards to meet: in natural photosynthesis, electrons and holes are generated from the initial CT state with near unit efficiency due to rapid charge separation (CS) versus extremely slow (∼1 s) charge recombination (CR).[6] The critical role of the CS-to-CR ratio in light-harvesting complexes[7,8] has inspired a substantial body of experimental and theoretical work on condensed phase CS and CR in small-molecule prototypes.[9−11]

Molecular polyads—consisting of a chromophore and one or several electron donors and acceptors—are a popular architecture for artificial light harvesting because they offer the potential for long-lived photoinduced CS in a small, chemically tunable package.[12−14] Triads,[15,16] tetrads,[17] and higher polyads, including dendrimeric structures,[18] exploit spatial separation of the terminal donor and acceptor to reduce the donor−acceptor electronic coupling, obtaining long-lived CT states at the expense of low yields of the CT state. Conversely, smaller dyads present high initial CT state yields, but fast geminate CR limits the overall efficiency of charge carrier generation.[19] How small the dyad can be while maintaining a capacity for photoinduced CS is an open and important question.

Given the daunting task of striking a favorable balance between CS and CR in these polyads, we anticipate further rational design and optimization to be contingent upon a mechanistic understanding of the underlying ET processes. The Marcus theory of ET[20,21] is an excellent guide in this respect. In Marcus theory, the ET rate is expressed in terms of three system-dependent parameters: the driving force ΔG, which is the free energy difference between the reactant and product states at equilibrium; the reorganization energy λ, which is the free energy cost to distort the configuration of the reactant to an equilibrium configuration of the product; and the donor−acceptor electronic coupling V_{DA}

$$k_{\mathrm{ET}} = \frac{2\pi}{\hbar} \frac{V_{\mathrm{DA}}^2}{\sqrt{4\pi\lambda k_{\mathrm{B}}T}} \exp\left[-\frac{(\lambda + \Delta G)^2}{4\lambda k_{\mathrm{B}}T}\right] \qquad (1)$$

The validity of the Marcus model has been thoroughly investigated and confirmed over a wide range of conditions,[22,23]

including the inverted region, $-\Delta G > \lambda$, where the ET rate is predicted to decrease with increasing driving force. The model assumes linear response of the bulk solvent polarization to the electric field. Several extensions have been proposed to account for situations where the model breaks down, for example, in systems with strong vibronic effects[24] or electronic state-dependent polarizabilities.[25] Marcus theory and its extensions provide a framework for correlating molecular structure with ET properties; thus, Marcus ET parameters are important for the analysis and refinement of molecular light-harvesting architectures.

Because of the experimental challenges associated with measuring ET parameters, especially the reorganization energy,[26,27] computer simulations have played an important role in developing an understanding of ET at the molecular level. These simulations present their own set of challenges. The role of the environment as a facilitator of ET has long been appreciated,[28,29] but the computational cost of modeling the environment from first-principles is often prohibitive. Instead, it is common to adopt a hybrid QM/MM model[30,31] in which the solute is described by a high-level electronic structure method while the solvent is treated with a classical force field. Furthermore, diabatic reactant and product states form a more suitable basis for studying ET than the adiabatic states obtained from traditional electronic structure methods.[32] Empirical valence-bond methods,[33] frozen-density functional theory,[34] and constrained density functional theory (CDFT)[35−37] have all been used to define diabatic states for ET simulations. While the complexity of these simulations has increased substantially over time, the accurate prediction of ET rates in solution remains unfinished business.

In this article, we characterize CR in the small molecular dyad formanilide−anthraquinone (FAAQ) in dimethylsulfoxide (DMSO) solution using a new QM/MM scheme for ET simulations. An unusually long-lived CT state was postulated for FAAQ in DMSO[38] on the basis of spectroscopic signatures which were later reassigned to a side reaction with the DMSO solvent.[39] The CT state is much shorter-lived in other solvents, so we naively expect fast CR in DMSO as well. Our simulations harnesses the power of CDFT to compute accurate diabatic states on the fly and the computational efficiency of polarizable force fields, achieving high-quality molecular dynamics (MD) sampling of the ET free energy surfaces. The simulations provide a detailed picture of the CR mechanism and confirm that CR in FAAQ is fast.

The rest of the article is organized as follows. First we introduce the compact donor−acceptor dyad FAAQ and review its experimental characterization in some detail. After highlighting the features we consider to be essential for a quantitative computational model of condensed phase ET free energies, we lay out the details of the simulations and present free energy profiles and ET parameters for the dyad in solution. Our model predicts ET parameters in line with experimental data and provides the first qualitatively correct prediction of the FAAQ reorganization energy in DMSO. Next we identify and characterize deviations from linear response in the simulations, and we show that torsional flexibility does not strongly modulate the CR rate in FAAQ. We then show that the energy gaps from the full simulations can be mapped quite well onto a simple electrostatic model of solvent polarization. Finally, we summarize strengths and weaknesses of our approach and suggest avenues for further applications and improvements.
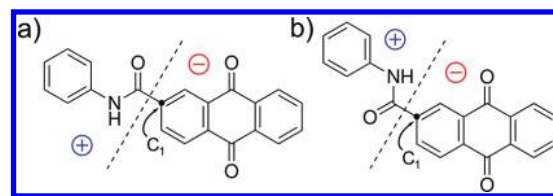

Figure 1. Structure of the FAAQ dyad in its (a) trans and (b) cis conformations. The dashed line indicates the location of the partition employed in this study between the donor (+) and acceptor (−).

■ MODEL SYSTEM: THE FAAQ DYAD

Solution phase ET in the FAAQ dyad,[38−41] shown in Figure 1, has been the subject of some controversy. The report of a CT excited state in FAAQ with a lifetime of nearly 1 ms[38] in DMSO contrasted sharply with the empirical rule-of-thumb that CR from singlet CT states in compact dyads generally takes place on picosecond time scales.[42] Later efforts to reproduce the long-lived CT state of FAAQ and to explore the dependence of its lifetime on solvent[39] concluded that the long-lived transient absorption signal previously assigned to the intramolecular CT state arises instead from intermolecular ET following photooxidation of DMSO. Femtosecond transient absorption studies on FAAQ in acetonitrile yielded more conventional CR rates of approximately 2 ps for the singlet CT state and 130 ns for the triplet CT state.[39]

Fortunately, the controversy has generated a wealth of experimental data for FAAQ. Electrochemical studies on FAAQ and related derivatives produced an estimate for the CR driving force,[38] $-\Delta G_{CR} = 2.24$ eV, later revised[39] to $-\Delta G_{CR} = 2.68$ eV. Both estimates are indirect deductions with unclear error bars, so we consider them useful qualitative guides, rather than absolute benchmarks, for comparison to our simulations. A rough estimate for the reorganization energy λ can also be found by comparing CT state lifetimes of FAAQ and its derivatives.[43] We first make the assumption that the difference in lifetimes τ of two polyads **A** and **B** is controlled by the difference in their activation free energies rather than the difference in their pre-exponential factors. This assumption is valid to the extent that the donor−acceptor coupling is similar for **A** and **B**; this may not be the case in the long-range ET regime where the coupling decays exponentially with donor−acceptor distance, but it is a more reasonable assumption for the modestly separated polyads considered here. Then the ratio of the CR lifetimes of **A** and **B** satisfies

$$\ln\left[\frac{\tau_{CR}(\mathbf{B})}{\tau_{CR}(\mathbf{A})}\right] = -\frac{\Delta G_{CR}^{\ddagger}(\mathbf{A}) - \Delta G_{CR}^{\ddagger}(\mathbf{B})}{k_B T}$$

$$\equiv -\frac{\Delta\Delta G_{CR}^{\ddagger}}{k_B T} \qquad (2)$$

where $\Delta G_{CR}^{\ddagger} = (\lambda + \Delta G_{CR})^2/(4\lambda)$ is the activation free energy for CR. Further assuming a negligible difference in the reorganization energy $\lambda(\mathbf{A}) = \lambda(\mathbf{B}) = \lambda$, we find

$$\lambda = \frac{\Delta(\Delta G_{CR})^2}{4\Delta\Delta G_{CR}^{\ddagger} - 2\Delta\Delta G_{CR}} \qquad (3)$$

We use experimentally determined lifetimes and driving forces for FAAQ and its ferrocenated derivative FcFAAQ ($\tau_{CR} = 20$ ps, $-\Delta G_{CR} = 1.16$ eV)[38] to estimate the reorganization energy.

12136

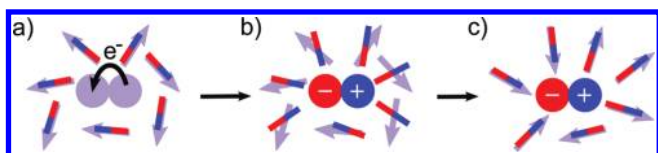dx.doi.org/10.1021/jp204962k |*J. Phys. Chem. B* 2011, 115, 12135–12144

Figure 2. Schematic of solvent reorganization associated with an ET event, highlighting electronic and orientational solvent polarization. Conjoined spheres represent the ET dyad; arrows represent the orientation of individual solvent molecules. (a) A spontaneous fluctuation of the solvent away from equilibrium facilitates an ET event. (b) Electronic polarization (red and blue bars) of the solvent in response to ET occurs much faster than (c) orientational polarization, eventually establishing equilibrium in the CT state.

Depending on the chosen estimate for $-\Delta G_{CR}$ in FAAQ, we obtain estimates of $\lambda = 1.53$ eV or $\lambda = 1.78$ eV. Finally, given the CT state lifetime of FAAQ and the estimates of ΔG_{CR} and λ, we can solve eq 1 for the electronic coupling to determine an estimated V_{DA} between 30 and 60 meV. These estimates provide a qualitative gauge for the integrity of our simulations within the framework of Marcus theory.

■ COMPUTATIONAL MODEL FOR ELECTRON TRANSFER

Any simulation of ET reactions requires a suitable definition of the reactant and product states. Among the many available definitions of diabatic states,[32,44] the CDFT approach is convenient because it retains the many advantages of Kohn–Sham DFT while also treating both diabatic states on the same footing.[45] This even-handed treatment is important because one of the diabatic states is often an excited state; it is especially crucial for CT excited states, which are often poorly described[46] by linear response time-dependent DFT (LR-TDDFT), the de facto standard tool for excited states in DFT.[47] CDFT avoids these complications by treating both diabatic states as ground states of modified potentials which constrain the net charge on the donor and acceptor to appropriate fixed values for each state.[35]

An appropriate solvent model is also crucial for accurate ET simulations. Unlike conventional chemical bond-breaking and bond-forming reactions, intramolecular ET in solution often proceeds from reactant to product state with negligible internal rearrangement; instead, the reaction is driven by solvent fluctuations,[48] as depicted in Figure 2. In the nonadiabatic limit (small V_{DA}), when a fluctuation brings the system to a configuration in which the reactant and product states have the same energy, an electron is transferred with probability proportional to V_{DA}^2.

In order to adequately characterize the solvent fluctuations, we require a solvent model which can capture both orientational and electronic polarization. These two effects operate on different time scales: the solvent electrons respond essentially instantaneously to changes in the electronic structure of the solute, while orientational and internal nuclear rearrangements of the solvent lag behind.[49,50] Dielectric continuum models offer a computationally efficient means of describing the dynamic solvent response, but these are typically limited to the linear response regime. Beyond linear response, atomistic models are the method of choice;[51,52] these models can capture nonlinear effects due to dependence of the solvent polarization on solute conformation or on the effective charge separation distance in the CT state.

Previous simulations on model systems have indicated that these effects can modify nonequilibrium properties like reorganization energies significantly.[53,54]

Based on the preceding considerations, we adopt a polarizable molecular mechanics (MMpol) model in which selected atoms in the solvent are endowed with isotropic polarizability by means of a charged particle (Drude oscillator) affixed by a fictitious spring.[55] Charges on the polarizable atoms are rescaled to compensate for the charges of the associated Drude oscillators. The solute, described with CDFT, is electronically embedded in the MMpol solvent, and the solute and solvent are allowed to polarize one another self-consistently. This CDFT/MMpol approach is designed to capture important solute/solvent interactions while remaining scalable to systems far beyond the computational capacity of a complete density functional approach. This scalability enables the simulation of asymmetrical ET reactions of flexible donor—acceptor systems in polar solvents, such as the FAAQ/DMSO system studied here.

■ COMPUTATIONAL DETAILS

All QM/MM calculations were carried out within the framework of the CHARMM/Q-Chem interface.[56−58] The QM subsystem, a single FAAQ molecule, was electronically embedded in a $34 \times 34 \times 34$ Å box of 314 DMSO molecules comprising the MM subsystem. The neutral (N) and charge transfer (CT) states of FAAQ were modeled using CDFT[35] with the B3LYP functional.[59] Energy gaps were computed with the 3-21G and 6-31G* basis sets, while the 3-21G basis was used exclusively for MD simulations in an effort to balance the conflicting goals of accurate energetics and long MD trajectories. The DMSO solvent was modeled using the all-atom force field of Strader and Feller,[60] modified to include electronic polarizability using Drude oscillators[55] bound to each heavy atom (C, O, S) of DMSO. The Drude particle polarizabilities were chosen to reproduce the dielectric constant of DMSO at optical frequencies ($\varepsilon_\infty = 2.19$), and the electrostatic point charges were scaled to 65% of their original values such that the zero-frequency dielectric constant was also reproduced ($\varepsilon_0 = 46.7$). The DMSO force field parameters and the details of our procedure for mutual polarization of solute and solvent can be found in the Supporting Information.

For MD simulations, all CH bonds in the DMSO solvent were constrained at their equilibrium length using the SHAKE algorithm[61] to help ensure energy conservation with a 2 fs time step. After an initial energy minimization, the FAAQ/DMSO system was equilibrated with NPT dynamics at 300 K and 1 atm. For the sake of efficiency, the system was first equilibrated using an all-MM model with customized force fields[62] for each of the two diabatic states of FAAQ, followed by further equilibration with the full polarizable QM/MM model. Several NVT polarizable QM/MM trajectories were then obtained, each multiple picoseconds in length, with FAAQ in either the neutral or CT electronic state. A simulation temperature of 300 K was enforced by a Nosé—Hoover thermostat. Data were collected only after 2 ps of equilibration for each trajectory. Equilibrium dynamics in the NVT ensemble samples the Helmholtz free energy A; however, the difference in the work term PV between the two diabatic states is expected to be negligible. Furthermore, the zero of free energy is arbitrary; therefore, we use the notation G for all simulated free energies to emphasize comparison with experiment.
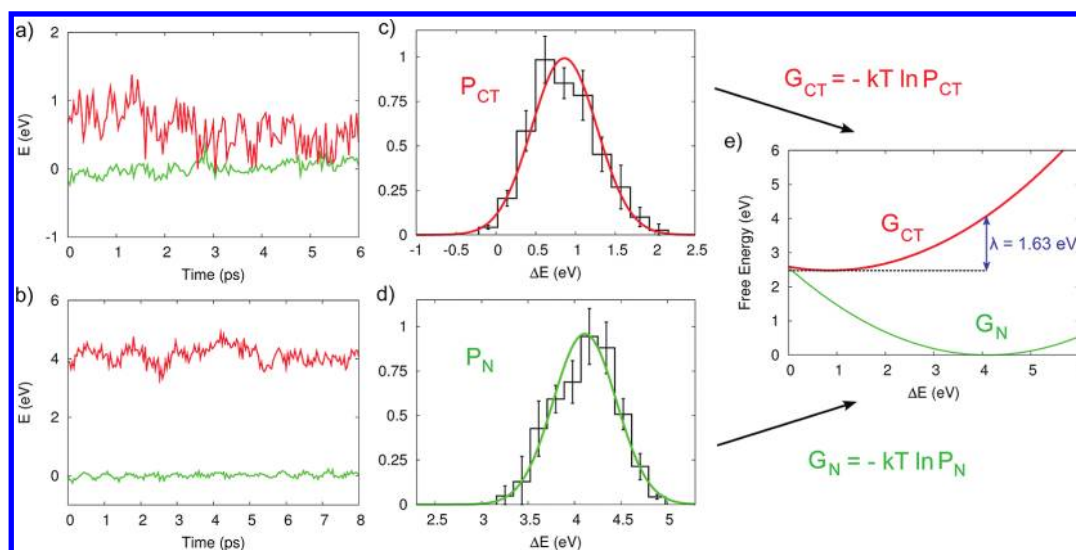
Figure 3. Construction of ET free energy curves for FAAQ. All energies are in eV. Several MD trajectories are computed with FAAQ either in the CT state (a) or the neutral state (b). Along each trajectory, the energy gap ΔE is sampled in order to generate probability distributions for the energy gap $P(\Delta E)$ for the (c) CT and (d) neutral trajectories. The histograms show the relative frequency of each energy gap window, while the curves are a Gaussian fit. (e) Free energy curves for the neutral and CT states are computed as the logarithm of the probability distributions.

Diabatic couplings were evaluated within the framework of CDFT,[63] both in the gas phase and in DMSO solvent. The solution phase couplings take into account the different solvation environments of the neutral and CT states by self-consistently polarizing each state's density with its own set of Drude particles prior to the coupling calculation. Solvent effects on CDFT couplings at the ET transition state were recently studied in the mixed-valence Q-TTF-Q anion in aqueous solution;[64] here we obtain complementary information about solvent effects on couplings for equilibrium configurations of both diabatic states. This data can be used to assess the validity of the Condon approximation in the FAAQ/DMSO system.[65]

■ RESULTS

Construction of Free Energy Profiles. As a first step toward determination of the ET free energy profiles, we obtained 30 ps of equilibrium polarizable QM/MM dynamics in each diabatic state (neutral or CT). A representative trajectory for each diabatic state is presented in parts a and b of Figure 3. Each plot also shows the energy of the other diabatic state at the various configurations visited along the trajectory.

We sample the vertical energy gap $\Delta E_\alpha = E_\alpha^{CT} - E_\alpha^{N}$ of configurations α at regular intervals of 40 fs along these trajectories to build up a statistical picture of the distribution of energy gaps, as illustrated in the histograms in Figure 3, parts c and d. The probability distribution of the energy gap in diabatic state X, $P_X(\Delta E)$, is related to the free energy G_X by

$$G_X(\Delta E) = -k_B T \ln P_X(\Delta E) \qquad (4)$$

where $P_X(\Delta E)$ is to be inferred from the energy gap histograms.

There are several reasonable ways to parametrize $P_X(\Delta E)$ from the sampled energy gaps. A Gaussian fit to the energy gap distribution will result in a parabolic free energy profile, in keeping with Marcus theory. However, there is no formal restriction on the functional form of the fit, provided it reasonably captures the statistical distribution of energy gaps. First, we

explore the Marcus picture, which facilitates comparison to the experimental ET parameters derived under the assumption of linear response. We then consider a more flexible model for the free energy and show that the predicted deviations from the Marcus model favor fast recombination of the CT state.

The Marcus Picture. Gaussian fits to the neutral and CT energy gap distributions are shown in parts c and d of Figure 3. The error bars in the histograms indicate the standard error in the bar heights obtained separately for each MD trajectory. Applying eq 4 to the Gaussian fits, we obtain the Marcus free energy curves in Figure 3e. The nested parabolas confirm that the simulations place CR in the Marcus inverted region, $-\Delta G_{CR} > \lambda$.

Within the linear response approximation, the driving force and reorganization energy can be obtained directly from the mean energy gaps of the neutral and CT configurations[26]
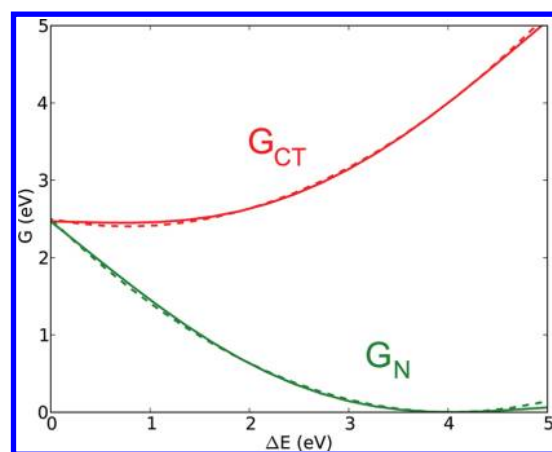
$$\Delta G_{CR} = \frac{1}{2}(\langle \Delta E \rangle_N + \langle \Delta E \rangle_{CT}) \qquad (5)$$

$$\lambda = \frac{1}{2}(\langle \Delta E \rangle_N - \langle \Delta E \rangle_{CT}) \qquad (6)$$

The mean energy gaps and corresponding ET parameters are presented in Table 1. Our ET parameters $\Delta G_{CR} = 2.38$ eV and $\lambda = 1.64$ eV fall between the two estimates inferred from experimental data, $-\Delta G_{CR} \approx 2.24-2.68$ eV and $\lambda \approx 1.53-1.78$ eV. From the standard error of the mean energy gap for each state, we estimate uncertainties of roughly 0.2 eV for both $-\Delta G_{CR}$ and λ due to the limited MD sampling. Nevertheless, the calculated $-\Delta G_{CR}$ and λ demonstrate that the experimental ET properties, interpreted within the Marcus picture, are borne out by the microscopic details of the CDFT/MMpol simulations. The agreement of our calculated λ with experiment is especially encouraging because it indicates that our simulations achieve a realistic picture of both equilibrium and nonequilibrium solvation regimes. Previous work has demonstrated that 0.2 eV of the reorganization energy arises directly from solute reorganization,[43] while an additional 0.6 eV can be attributed to bulk electrostatic effects.[32] The larger reorganization energy found

Table 1. ET Parameters Obtained from MD Simulations, Assuming Gaussian Statistics for the Energy Gap[a]

basis set	$\langle \Delta E \rangle_N$	$\langle \Delta E \rangle_{CT}$	$-\Delta G_{CR}$	λ_{CR}	$\Delta G_{CR}^{\ddagger}$
3-21G	4.13	0.86	2.49	1.63	0.11
6-31G*	4.03	0.74	2.38	1.64	0.08

[a] All energies are in eV.

Table 2. CR Parameters Obtained under the Linear Response Approximation and under the Quartic Fits[a]

approximation	σ_N	σ_{CT}	$-\Delta G_{CR}$	λ_{CR}	$\Delta G_{CR}^{\ddagger}$
linear response	0.29	0.29	2.38	1.64	0.08
nonlinear correction	0.35	0.43	2.45	1.58	0.02

[a] All energies are in eV.

Figure 4. Quartic parametrization of the neutral and CT free energy profiles (solid lines). Marcus free energy profiles (dashed lines) are shown for comparison.

here suggests that solvent configurations at equilibrium with either diabatic state are further stabilized, relative to nonequilibrium configurations, by conformation-specific solute–solvent interactions such as hydrogen bonding that are not captured by conventional continuum solvent approaches.[66]

Beyond Linear Response. Having validated the Marcus picture obtained through the CDFT/MMpol approach, we can investigate the degree to which the simulations predict deviations from the linear response regime in the FAAQ/DMSO ET reaction. The linear response assumption is built into most implicit solvent models,[67] so CDFT/MMpol is specially poised to probe this question.

We begin by observing that our simulations do not provide a statistically even-handed description of the entire reaction coordinate: the sampling is most complete in the vicinity of the neutral and CT free energy minima. An umbrella sampling approach could overcome this limitation[68] and should provide an interesting avenue for further investigation. Here, we focus on the statistics of the energy gap near the free energy minima.

In the last section, ensemble-averaged energy gaps were used to compute ET parameters via eq 5 and eq 6. However, in addition to the average energy gaps, our simulations provide an estimate of typical fluctuations σ_X of the energy gap. Linear response dictates that both diabatic states experience the same energy gap fluctuations, but the simulations do not fully bear out this assumption. We find markedly larger energy gap fluctuations for the CT state, $\sigma_{CT} = 0.43$ eV, compared to the neutral state fluctuations, $\sigma_N = 0.35$ eV. We performed two statistical tests of the hypothesis that the collection of energy gaps for the neutral and CT diabatic states came from distributions with the same variance. The traditional F-test and Levene's test[69] both reject the null hypothesis of equal variances ($p < 0.01$).

What are the mechanistic and kinetic consequences of the nonlinear solvent response? To address this key question, we used the four statistics—energy gap averages and fluctuations for each state—to obtain a unique quartic parametrization of the neutral free energy curve (up to an arbitrary choice of the zero of free energy)

$$G_N(q) = G_0 + G_1 q + \frac{1}{2}G_2 q^2 + \frac{1}{6}G_3 q^3 + \frac{1}{24}G_4 q^4 \quad (7)$$

where $q = \Delta E - \langle \Delta E \rangle_N$. From eq 7, a quartic expression for G_{CT} is uniquely obtained via the linear free energy relation,[70] $G_{CT}(\Delta E) = G_N(\Delta E) + \Delta E$. The same overall fit is obtained regardless of which state is parametrized first. Expressions for the coefficients G_i in terms of $\langle \Delta E \rangle_N$, $\langle \Delta E \rangle_{CT}$, σ_N, and σ_{CT} can be found in the Supporting Information.

The quartic free energy model is displayed in Figure 4. Qualitatively, the quartic fit is strikingly similar to the Marcus picture. Nevertheless, the nonlinear solvent response raises the driving force by 0.07 eV to $-\Delta G_{CR} = 2.45$ eV and lowers the reorganization energy by 0.06 eV to $\lambda_{CR} = 1.58$ eV. As shown in Table 2, the activation barrier to CR is significantly reduced in the quartic model to $\Delta G_{CR}^{\ddagger} = 0.02$ eV. From the ratio of $\Delta G_{CR}^{\ddagger}$ for the Marcus and quartic models, the quartic model predicts an order-of-magnitude enhancement of k_{CR} relative to the Marcus picture. This finding emphasizes that slight nonlinearities in the solvent response—which have been characterized experimentally in other examples of condensed phase ET[71,72]—can fundamentally alter the kinetics of CR and CS.

Characterization of the Electronic Coupling. The Marcus expression, eq 1, has a standard interpretation from the perspective of classical transition state theory:[73] the exponential term, parametrized by the reorganization energy and driving force for ET, embodies the likelihood of visiting the transition state region where an ET event becomes maximally probable; then the pre-exponential term, controlled by the electronic coupling, characterizes the inherent probability of ET at the isoenergetic point. In the last section, we used the diagonal elements of the diabatic two-state Hamiltonian to compute energy gap fluctuations and parametrize the exponential term in the rate expression; here, we use CDFT to characterize V_{DA} as well as its fluctuations in the neutral and CT ensembles.

The magnitude of the CDFT couplings, presented in Table 3, is in excess of most experimentally determined couplings for compact donor–acceptor dyads.[42] The couplings also exceed our previously described estimate $V_{DA} \approx 0.03–0.06$ eV by an order of magnitude. We anticipate that much of the discrepancy between the computed and experimentally inferred couplings can be attributed to the short-range character of intramolecular ET in FAAQ. In most systems for which the CDFT coupling prescription has been tested and validated, the relevant ET process is either intermolecular[74] or bridge-mediated.[75,76] In FAAQ, the donor–acceptor "bridge" is effectively a single C–C bond; this feature makes the CDFT coupling especially sensitive

Table 3. Mean Electronic Couplings and Deviations for Neutral and CT Configurations of FAAQ in the Gas Phase and in DMSO Solution[a]

configurations	$\langle V_{DA} \rangle$	σ_V
Gas Phase		
neutral	0.90	0.15
CT	0.73	0.18
DMSO		
neutral	0.61	0.12
CT	0.25	0.06

[a] All energies are in eV.

to the size and shape of the constraints. Nevertheless, these errors should be largely systematic across the sampled configurations because the same partitioning strategy was used for all configurations. Therefore we can still gain mechanistic insights by studying trends in the CDFT couplings.

The distribution of electronic couplings presented in Table 3 reveals several interesting trends. First, the neutral configurations exhibit a substantially larger coupling than the CT configurations, indicative of a modest non-Condon effect.[65,77] In particular, the observation of increased electronic coupling for configurations exhibiting a larger energy gap indicates that the mean electronic coupling at the transition state $\Delta E = 0$, where its magnitude matters most, may be smaller than the values predicted here.

Another striking feature of the couplings is the substantial difference between the gas phase and solution phase values, both for mean couplings and for deviations. Other recent simulations of solvent effects on electronic couplings[64,75,78,79] have been at odds regarding the magnitude of these effects; here we find a significant reduction of the coupling matrix element upon incorporation of solvent. Fluctuations in the coupling are also damped by the solvent, as was also observed in a computational study where the time dependence of V_{DA} was monitored explicitly.[80]

Finally, we note that the ET parameters obtained from our simulations correspond to CT state lifetimes on the femtosecond to picosecond time scale, in qualitative agreement with the experimental refutation[39] of the previously claimed long-lived CT state in FAAQ.[38] Future fine-tuning of the CDFT coupling prescription should lead to improved estimates of the coupling, thereby enabling quantitative ET rate calculations within the CDFT/MMpol model.

■ DISCUSSION

The use of the diabatic energy gap as a reaction coordinate for solution phase ET has a long history rooted in Warshel's semiclassical trajectory approach.[81,82] This particular choice of reaction coordinate is convenient because it collapses the full complexity of the solvent dynamics onto a single degree of freedom, while still providing a quadratic free energy profile in the limit of linear response.[83] The energy gap is also easier to control for the purposes of umbrella sampling than other more physically appealing choices such as a solvent polarization reaction coordinate, motivated by the original work of Marcus.[20]

But the physical content of ΔE as a reaction coordinate is limited. How does the reaction proceed? First we consider the extent to which a key internal degree of freedom in FAAQ, the dihedral angle between the donor and acceptor, influences the
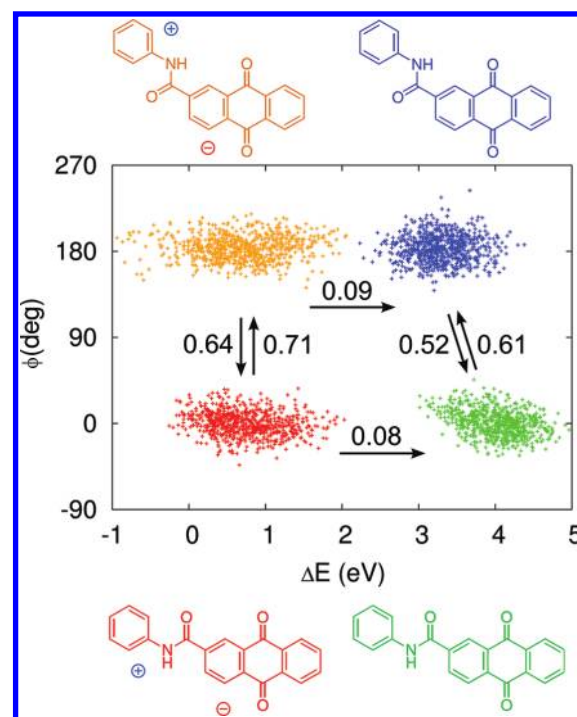

Figure 5. Scatter plot of the energy gap ΔE and dihedral angle ϕ for snapshots from all MD trajectories. Colors represent the type of snapshot: green = neutral, trans; red = CT, trans; blue = neutral, cis; orange = CT, cis. The labeled arrows indicate activation energies $\Delta G^{\ddagger}$ (in eV) for transitions between the four wells ($\uparrow$, $\downarrow$: cis–trans isomerization; $\rightarrow$: charge recombination).

ET free energy profiles. Could excited state isomerization have a measurable effect on k_{CR}? We then turn our attention to the role of the solvent and to the notion of a collective solvent coordinate for ET in particular. Toward this end, we map the diabatic energy gaps from our simulations onto a classical polarization coordinate. The correlation between the energy gap and the polarization coordinate provides another measure of how successfully the Marcus model captures the atomistic details of our simulations.

Role of Solute Flexibility in ET Kinetics. The FAAQ molecule is highly conjugated, with the amide bridge providing the only practical means of breaking planarity. The torsional barrier between the FA and AQ groups is expected to be large compared to $k_B T$, prohibiting any substantial population of the cis configurations illustrated in Figure 1b. Nevertheless, the possibility of photoinduced isomerization prompted us to examine whether the cis and trans configurations have different ET kinetics, and if so, to quantify the difference.

We obtained 750 snapshots of cis configurations for each diabatic state, following the same procedure outlined for the trans configurations. To obtain a rough estimate of the free energy of activation for isomerization, we take the linear response approach and fit the statistics of the dihedral angle ϕ to a pair of parabolas

$$G_{cis}(\phi) = \frac{1}{2\sigma_{cis}^2}(\phi - \langle\phi\rangle_{cis})^2 \tag{8}$$

$$G_{trans}(\phi) = \frac{1}{2\sigma_{trans}^2}(\phi - \langle\phi\rangle_{trans})^2 + \Delta G_{cis-trans} \tag{9}$$

The free energy difference $\Delta G_{cis-trans} = G_{cis}(\langle\phi\rangle_{cis}) - G_{trans}(\langle\phi\rangle_{trans})$ was approximated from the free energy of optimized cis and trans

FAAQ structures obtained at the B3LYP/6-31G* level with DMSO modeled by the SM8 model,[84] yielding $\Delta G_{cis-trans}$ = 3.8 meV. Then we estimate the free energy barrier to isomerization by computing the free energy at the curve-crossing.

Activation free energies for isomerization and for CR within the linear response approximation are shown in Figure 5, super-imposed over the distribution of all 3000 snapshots in the (ΔE, ϕ) plane. The isomerization barrier heights range from 0.52 to 0.71 eV (12 to 16 kcal mol^{-1}); given the short lifetime of the CT state, these barriers preclude any substantial degree of excited state isomerization. We therefore expect that any influence of the cis isomer on the overall CR rate in experiments can be safely neglected. Furthermore, the barrier heights for CR within the Marcus picture are quite similar for the two isomers: 0.08 (0.09) eV for CR in the cis (trans) conformation. Thus, even if isomerization were more facile, it would have only a minor influence on k_{CR}.

In summary, the linear response assumption leads to a model for the ET mechanism in which CR is largely decoupled from cis—trans isomerization. The rigidity of the donor and acceptor units precludes any further dependence of the CR rate on the details of solute conformation. These insights raise the possibility of constructing an ET reaction coordinate that captures the key solute—solvent interactions while averaging out all of the internal degrees of freedom in FAAQ. We explore this possibility next.

Reaction Coordinate Based on a Simplified Electrostatic Model. How well can a classical solvent polarization coordinate capture the atomistic details of the ET simulations? To provide a quantitative answer, we construct a plausible polarization co-ordinate and study its correlation with the energy gap reaction coordinate.

We express the collective solvent polarization in terms of an *electrostatic* energy gap possessing the general form $\Delta E_{el} = \Delta(\mu_X \cdot \mathbf{E}_X)$, where μ_X is the electric dipole moment of FAAQ in diabatic state X, and $\mathbf{E}_X$ is the electric field generated by the particular solvent configuration around the solute dipole. The construction of ΔE_{el} is outlined below; further details are available in the Supporting Information.

First we replace the FAAQ dyad with a point electric dipole μ_X whose magnitude and direction are fixed to reproduce the ensemble-averaged dipole moment of FAAQ in diabatic state X, as obtained from our simulations. The DMSO solvent is treated as a collection of point charges, taken directly from the MM model. Then the electrostatic energy gap for a given snapshot α is the difference between the interaction energies of the solute dipole and solvent electric field in the two diabatic states

$$\Delta E_{el} = \langle u \rangle_{CT} \cdot \mathbf{E}_{CT} - \langle u \rangle_N \cdot \mathbf{E}_N \qquad (10)$$

Given this prescription, we evaluate ΔE_{el} for snapshots α from the CDFT/MMpol simulations and consider the correlation r between ΔE_{el} and the diabatic energy gap ΔE

$$r \equiv \mathrm{Corr}(\Delta E, \Delta E_{el})$$

$$= \frac{1}{N-1} \sum_{\alpha=1}^{N} \left(\frac{\Delta E_\alpha - \langle \Delta E \rangle}{\sigma_{\Delta E}} \right) \left(\frac{\Delta E_{el,\alpha} - \langle \Delta E_{el} \rangle}{\sigma_{\Delta E_{el}}} \right) \qquad (11)$$

The location of the solute dipole in the definition of ΔE_{el} remains to be determined; two possibilities are considered here. First, to set an upper bound on the correlation achievable with a single-dipole representation of FAAQ, we placed a dipole at each nucleus i of the molecule and considered the linear combination $\mu = \sum_i c_i \mu_i$. The correlation coefficient r in this model can then be
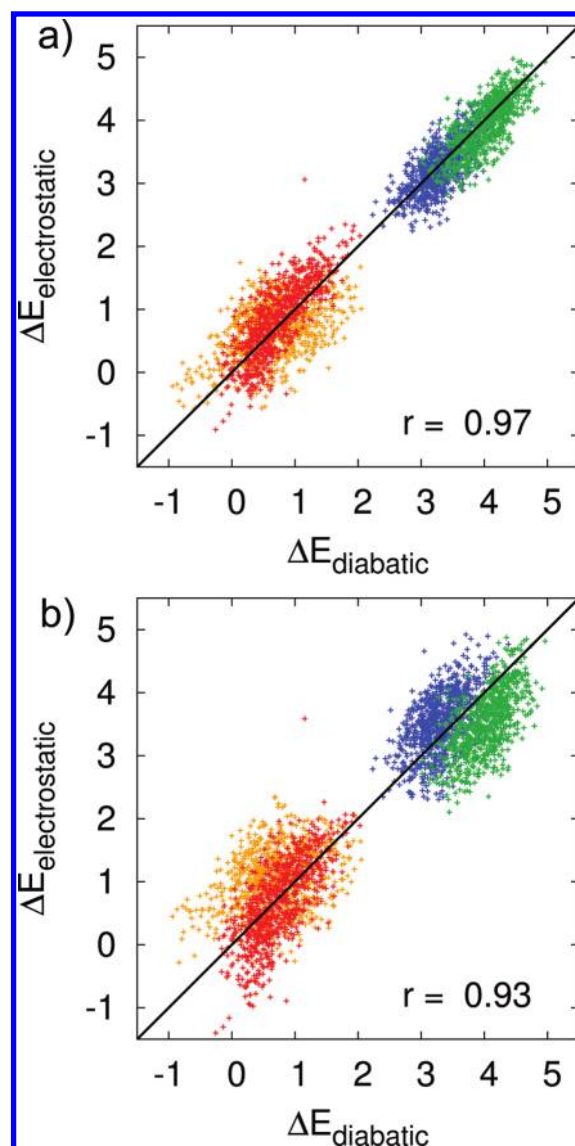

Figure 6. Correlation between the diabatic energy gap and electrostatic energy gap, where the latter describes the interaction between the solvent electric field and (a) a linear combination of dipoles at each FAAQ nucleus or (b) a single dipole placed at C_1 (see Figure 1). Colors represent the type of snapshot: green = neutral, trans; red = CT, trans; blue = neutral, cis; orange = CT, cis.

optimized with respect to the coefficients **c** in a least-squares sense.[85] This model has 38 degrees of freedom (one per nucleus in the FAAQ model) and achieves a correlation r = 0.97 upon optimization of **c** as illustrated in Figure 6a.

The correlation is reduced slightly when we restrict the model of the solute to a single dipole. Varying the location of the single dipole over all FAAQ nuclei, we obtained an optimal correlation r = 0.93 (Figure 6b) by placing it on the carbon atom labeled C_1 in Figure 1. Thus, we can account for the bulk of the energy gap fluctuations in the FAAQ/DMSO system with a simple electro-static model of solvent polarization.

The correlation scatter plots in Figure 6 show some interesting trends. First, the polarization models provide a better fit for the neutral configurations than for the CT configurations, likely because of the more drastic difference in polarization between

12141

dx.doi.org/10.1021/jp204962k |*J. Phys. Chem. B* 2011, 115, 12135–12144

the two diabatic states at neutral configurations. Also, the cis and trans isomers are segregated in the single-dipole scatter plot in Figure 6b. The two isomers have different effective charge separation distances in the CT state, so it is sensible that the best-fit mappings between ΔE and ΔE_{el} for the cis and trans configurations could have different constant shifts. The inclusion of additional solute degrees of freedom can mask the distinction between the isomers, as evidenced by the lack of isomer segregation in Figure 6a.

Some potentially important features that our simulations cannot intrinsically capture, such as intermolecular charge transfer between the solute and the first solvation shell[86] or within the solvent,[87] are naturally absent from this analysis. Still, the scatter plots show that solvent polarization coordinates can be constructed which faithfully mirror the energy gaps obtained from the full CDFT/MMpol simulations.

■ CONCLUSION

We have explored the mechanistic and kinetic details of ET in the compact donor—acceptor dyad FAAQ solvated in DMSO. Our simulations corroborate experimental evidence that CR takes place in the Marcus inverted region. Although inverted region effects have been postulated to drastically extend the lifetimes of singlet CT excited states in compact dyads,[38] we find a small activation barrier that promotes CR on the picosecond time scale, in agreement with transient absorption studies.[39] A modest nonlinear solvent response further enhances the CR rate.

From the microscopic details of the simulations, we identify several mechanistic features bearing consequences for the ET kinetics. We find evidence of non-Condon effects: the electronic coupling is weaker in the equilibrium solvation environment of the CT state than in that of the ground state. Cis—trans isomerization does not appear to qualitatively change the ET landscape in FAAQ. Finally, we find good correlation between the diabatic energy gap and a simplified electrostatic reaction coordinate. Despite signatures of nonlinear response detected in our simulations, the Marcus picture of ET driven by collective solvent polarization captures the fundamental mechanism of CR in FAAQ.

To carry out these simulations, we have introduced a computational model, CDFT/MMpol, for condensed phase ET simulations. Designed for accuracy and scalability, the CDFT/MMpol approach couples diabatic states from constrained DFT with a polarizable force field to account for mutual polarization of the donor—acceptor system and surrounding solvent. A more accurate modeling of the solute—solvent interaction—for example, at a QM/QM level—would serve to shore up our evidence of a nonlinear response; but obtaining sufficient statistics to demonstrate the effect at a higher level of theory would make such an effort intractably demanding from a computational standpoint.

Looking ahead, the approach outlined here is readily adaptable to the presence of other low-lying excited states, for example, the localized S_1 state on AQ from which CS originates in FAAQ. These states can be treated with DFT methods better suited to localized excitations, such as LR-TDDFT[47,88] or ΔSCF.[89,90] Together with a prescription for couplings between CT and local excited states,[91] this approach would provide a fully self-consistent model of CR *and* CS in the condensed phase. Such a model would represent an important step toward predicting how the ratio of CS to CR might be tuned through chemical modifications.

To extend the scope of the CDFT/MMpol approach to larger polyads such as donor—bridge—fullerene systems[92,93] or to models of natural photosynthesis,[94,95] it would be appealing to substitute the CDFT description of the solute with an accurate MMpol model for configurational sampling.[74] Improvements in force-matching techniques are cause for optimism that MMpol force fields can rise to this challenge.[62]

Finally, we anticipate that CDFT/MMpol will provide a useful starting point for real-time quantum or semiclassical dynamics simulations of condensed phase ET.[96,97] These methods require diabatic energies and couplings along real-time trajectories; our approach can supply the necessary parameters on-the-fly for ET in complex systems. We look forward to applying CDFT/MMpol simulations to existing and nascent formulations of real-time ET dynamics such as the two-hop Langevin equation recently proposed by our group.[98]

■ ASSOCIATED CONTENT

S Supporting Information. Additional computational details; quartic free energy expressions; details of the electrostatic energy gap model; polarizable DMSO force field parameters; complete refs 1, 56, and 57. This material is available free of charge via the Internet at http://pubs.acs.org/.

■ AUTHOR INFORMATION

Corresponding Author
*E-mail: tvan@mit.edu.

■ ACKNOWLEDGMENT

■ REFERENCES

(1) Ham, M.-H.; et al. *Nat. Chem.* **2010**, *2*, 929–936.
(2) McConnell, I.; Li, G. H.; Brudvig, G. W. *Chem. Biol.* **2010**, *17*, 434–447.
(3) Grätzel, M. *Nature* **2001**, *414*, 338–344.
(4) D., V.; Ipek, O.; Meskers, S. C. J.; Sweelssen, J.; Koetse, M. M.; Veenstra, S. C.; Kroon, J. M.; van Bavel, S. S.; Loos, J.; Janssen, R. A. J. *J. Am. Chem. Soc.* **2008**, *130*, 7721–7735.
(5) Lee, J.; Vandewal, K.; Yost, S.; Bahlke, M. E.; Goris, L.; Baldo, M. A.; Manca, J. V.; Van Voorhis, T. *J. Am. Chem. Soc.* **2010**, *132*, 11878–11880.
(6) Blankenship, R. E. *Molecular Mechanisms of Photosynthesis*; Blackwell Science: Oxford, U.K., 2002.
(7) Hagfeldt, A.; Gratzel, M. *Acc. Chem. Res.* **2000**, *33*, 269–277.
(8) Mauer, R.; Howard, I. A.; Laquai, F. *J. Phys. Chem. Lett.* **2010**, *1*, 3500–3505.
(9) Barbara, P. F.; Meyer, T. J.; Ratner, M. A. *J. Phys. Chem.* **1996**, *100*, 13148–13168.
(10) Wasielewski, M. R.; Niemczyk, M. P.; Svec, W. A.; Pewitt, E. B. *J. Am. Chem. Soc.* **1985**, *107*, 1080–1082.
(11) Liu, T.; Troisi, A. *J. Phys. Chem. C* **2011**, *115*, 2406–2415.
(12) Imahori, H.; Tamaki, K.; Guldi, D. M.; Luo, C. P.; Fukitsuka, M.; Ito, O.; Sakata, Y.; Fukuzumi, S. *J. Am. Chem. Soc.* **2001**, *123*, 2607–2617.
(13) Hoppe, H.; Sariciftci, N. S. *J. Mater. Res.* **2004**, *19*, 1924–1945.

12142

dx.doi.org/10.1021/jp204962k |*J. Phys. Chem. B* 2011, 115, 12135–12144

(14) Lloyd, M. T.; Anthony, J. E.; Malliaras, G. G. *Mater. Today* **2007**, *10*, 34–41.

(15) Gouloumis, A.; de la Escosura, A.; Vazquez, P.; Torres, T.; Kahnt, A.; Guldi, D. M.; Neugebauer, H.; Winder, C.; Drees, M.; Sariciftci, N. S. *Org. Lett.* **2006**, *8*, 5187–5190.

(16) Xamena, F. X. L. I.; Teruel, L.; Alvaro, M.; Garcia, H. *Chem.— Eur. J.* **2007**, *13*, 515–519.

(17) Hasharoni, K.; Levanon, H.; Tang, J.; Bowman, M. K.; Norris, J. R.; Gust, D.; Moore, T. A.; Moore, A. L. *J. Am. Chem. Soc.* **1990**, *112*, 6477–6481.

(18) Satoh, N.; Nakashima, T.; Yamamoto, K. *J. Am. Chem. Soc.* **2005**, *127*, 13030–13038.

(19) Verhoeven, J. W.; van Ramesdonk, H. J.; Groeneveld, M. M.; Benniston, A. C.; Harriman, A. *ChemPhysChem* **2005**, *6*, 2251–2260.

(20) Marcus, R. A. *J. Chem. Phys.* **1956**, *24*, 966–978.

(21) Marcus, R. A. *Annu. Rev. Phys. Chem.* **1964**, *15*, 155–196.

(22) Miller, J. R.; Beitz, J. V.; Huddleston, R. K. *J. Am. Chem. Soc.* **1984**, *106*, 5057–5068.

(23) Clegg, A. D.; Rees, N. V.; Klymenko, O. V.; Coles, B. A.; Compton, R. G. *ChemPhysChem* **2004**, *5*, 1234–1240.

(24) Jortner, J. *J. Chem. Phys.* **1976**, *64*, 4860–4867.

(25) Small, D. W.; Matyushov, D. V.; Voth, G. A. *J. Am. Chem. Soc.* **2003**, *125*, 7470–7478.

(26) Blumberger, J. *Phys. Chem. Chem. Phys.* **2008**, *10*, 5651–5667.

(27) Tipmanee, V.; Oberhofer, H.; Park, M.; Kim, K. S.; Blumberger, J. *J. Am. Chem. Soc.* **2010**, *132*, 17032–17040.

(28) Warshel, A. *J. Phys. Chem.* **1982**, *86*, 2218–2224.

(29) Kuharski, R. A.; Bader, J. S.; Chandler, D.; Sprik, M.; Klein, M. L.; Impey, R. W. *J. Chem. Phys.* **1988**, *89*, 3248–3257.

(30) Warshel, A.; Levitt, M. *J. Mol. Biol.* **1976**, *103*, 227–249.

(31) Olsson, M. H. M.; Hong, G. Y.; Warshel, A. *J. Am. Chem. Soc.* **2003**, *125*, 5025–5039.

(32) Van Voorhis, T.; Kowalczyk, T.; Kaduk, B.; Wang, L.-P.; Cheng, C.-L.; Wu, Q. *Annu. Rev. Phys. Chem.* **2010**, *61*, 149–170.

(33) Warshel, A.; Weiss, R. M. *J. Am. Chem. Soc.* **1980**, *102*, 6218–6226.

(34) King, G.; Warshel, A. *J. Chem. Phys.* **1990**, *93*, 8682–8692.

(35) Wu, Q.; Van Voorhis, T. *Phys. Rev. A* **2005**, *72*, 024502.

(36) Sit, P. H.-L.; Cococcioni, M.; Marzari, N. *Phys. Rev. Lett.* **2006**, *97*, 028303.

(37) Oberhofer, H.; Blumberger, J. *J. Chem. Phys.* **2009**, *131*, 064101.

(38) Okamoto, K.; Hasobe, T.; Tkachenko, N. V.; Lemmetyinen, H.; Kamat, P. V.; Fukuzumi, S. *J. Phys. Chem. A* **2005**, *109*, 4662–4670.

(39) Van Ramesdonk, H. J.; Bakker, B. H.; Groeneveld, M. M.; Verhoeven, J. W.; Allen, B. D.; Rostron, J. P.; Harriman, A. *J. Phys. Chem. A* **2006**, *110*, 13145–13150.

(40) Hamanoue, K.; Nakayama, T.; Nanshow, H.; Hanada, T.; Naruta, Y.; Kodo, T.; Maruyama, K. *J. Chem. Soc., Faraday Trans.* **2003** , *89*, 3243–3250.

(41) Allen, N. S.; Pullen, G.; Shah, M.; Edge, M.; Holdsworth, D.; Weddell, I.; Swart, R.; Catalina, F. *J. Photochem. Photobiol., A* **1995**, *91*, 73–79.

(42) Verhoeven, J. W. *J. Photochem. Photobiol., C* **2006**, *7*, 40–60.

(43) Wu, Q.; Van Voorhis, T. *J. Phys. Chem. A* **2006**, *110*, 9212–9218.

(44) Subotnik, J. E.; Cave, R. J.; Steele, R. P.; Shenvi, N. *J. Chem. Phys.* **2009**, *130*, 234102.

(45) Wu, Q.; Van Voorhis, T. *J. Chem. Theory Comput.* **2006**, *2*, 765–774.

(46) Dreuw, A.; Head-Gordon, M. *J. Am. Chem. Soc.* **2004**, *126*, 4007–4016.

(47) Dreuw, A.; Head-Gordon, M. *Chem. Rev.* **2005**, *105*, 4009–4037.

(48) Kosower, E. M.; Huppert, D. *Chem. Phys. Lett.* **1983**, *96*, 433–435.

(49) Kim, H. J.; Hynes, J. T. *J. Chem. Phys.* **1990**, *93*, 5194–5200.

(50) Aguilar, M. A. *J. Phys. Chem. A* **2001**, *105*, 10393–10396.

(51) Warshel, A.; Parson, W. W. *Annu. Rev. Phys. Chem.* **1991**, *42*, 279–309.

(52) Simonson, T. *Proc. Natl. Acad. Sci. U.S.A.* **2002**, *99*, 6544–6549.

(53) Matyushov, D. V.; Voth, G. A. *J. Chem. Phys.* **2000**, *113*, 5413–5424.

(54) Ishida, T. *J. Phys. Chem. B* **2005**, *109*, 18558–18564.

(55) Lamoureux, G.; Roux, B. *J. Chem. Phys.* **2003**, *119*, 3025–3039.

(56) Brooks, B. R.; et al. *J. Comput. Chem.* **2009**, *30*, 1545–1614.

(57) Shao, Y.; et al. *Phys. Chem. Chem. Phys.* **2006**, *8*, 3172–3191.

(58) Woodcock, H. L.; Hodoscek, M.; Gilbert, A. T. B.; Gill, P. M. W.; Schaefer, H. F., III; Brooks, B. R. *J. Comput. Chem.* **2007**, *28*, 1485–1502.

(59) Becke, A. D. *J. Chem. Phys.* **1993**, *98*, 5648–5652.

(60) Strader, M. L.; Feller, S. E. *J. Phys. Chem. A* **2002**, *106*, 1074–1080.

(61) Ryckaert, J.-P.; Ciccotti, G.; Berendsen, H. J. C. *J. Comput. Phys.* **1977**, *23*, 327–341.

(62) Wang, L.-P.; Van Voorhis, T. *J. Chem. Phys.* **2010**, *133*, 231101.

(63) Wu, Q.; Van Voorhis, T. *J. Chem. Phys.* **2006**, *125*, 164105.

(64) Oberhofer, H.; Blumberger, J. *J. Chem. Phys.* **2010**, *133*, 244105.

(65) Toutounji, M. M.; Ratner, M. A. *J. Phys. Chem. A* **2000**, *104*, 8566–8569.

(66) Hu, H.; Yang, W. *J. Phys. Chem. B* **2010**, *114*, 2755–2759.

(67) Cramer, C. J.; Truhlar, D. G. *Chem. Rev.* **1999**, *99*, 2161–2200.

(68) Torrie, G. M.; Valleau, J. P. *J. Comput. Phys.* **1977**, *23*, 187–199.

(69) Levene, H. In *Contributions to Probability and Statistics: Essays in Honor of Harold Hotelling*; Olkin, I., Ed.; Stanford University Press, Palt Alto, CA, 1960; pp 278−292.

(70) Tachiya, M. *J. Phys. Chem.* **1989**, *93*, 7050–7052.

(71) Underwood, D. F.; Blank, D. A. *J. Phys. Chem. A* **2005**, *109*, 3295–3306.

(72) Bragg, A. E.; Cavanagh, M. C.; Schwartz, B. J. *Science* **2008**, *321*, 1817–1822.

(73) Eyring, H. *J. Chem. Phys.* **1935**, *3*, 107–115.

(74) Difley, S.; Wang, L.-P.; Yeganeh, S.; Yost, S.; Van Voorhis, T. *Acc. Chem. Res.* **2010**, *43*, 995–1004.

(75) Ding, F.; Wang, H.; Wu, Q.; Van Voorhis, T.; Chen, S.; Konopelski, J. *J. Phys. Chem. A* **2010**, *114*, 6039–6046.

(76) Yeganeh, S.; Van Voorhis, T. *J. Phys. Chem. C* **2010**, *114*, 20756–20763.

(77) Skourtis, S. S.; Waldeck, D. H.; Beratan, D. N. *Annu. Rev. Phys. Chem.* **2010**, *61*, 461–485.

(78) Hong, G.; Rosta, E.; Warshel, A. *J. Phys. Chem. B* **2006**, *110*, 19570–19574.

(79) Wallrapp, F.; Voityuk, A.; Guallar, V. *J. Chem. Theory Comput.* **2009**, *5*, 3312–3320.

(80) Troisi, A.; Ratner, M. A.; Zimmt, M. B. *J. Am. Chem. Soc.* **2004**, *126*, 2215–2224.

(81) Warshel, A.; Hwang, J. K. *J. Chem. Phys.* **1986**, *84*, 4938–4957.

(82) Hwang, J.-K.; Warshel, A. *J. Am. Chem. Soc.* **1987**, *109*, 715–720.

(83) Rasaiah, J. C.; Zhu, J. *J. Chem. Phys.* **2008**, *129*, 214503.

(84) Marenich, A. V.; Olson, R. M.; Kelly, C. P.; Cramer, C. J.; Truhlar, D. G. *J. Chem. Theory Comput.* **2007**, *3*, 2011–2033.

(85) Mahata, K.; Mahata, P. Proceedings of the 2007 15th International Conference on Digital Signal Processing, New York, 2007; pp 107−110.

(86) Bulo, R. E.; Ensing, B.; Sikkema, J.; Visscher, L. *J. Chem. Theory Comput.* **2009**, *5*, 2212–2221.

(87) Chen, J.; Martínez, T. J. *Chem. Phys. Lett.* **2007**, *438*, 315–320.

(88) Marques, M. A. L.; Gross, E. K. U. *Annu. Rev. Phys. Chem.* **2004**, *55*, 427–455.

(89) Ziegler, T.; Rauk, A.; Baerends, E. J. *Theor. Chim. Acta* **1977**, *43*, 261–271.

(90) Kowalczyk, T.; Yost, S. R.; Van Voorhis, T. *J. Chem. Phys.* **2011**, *134*, 054128.

(91) Difley, S.; Van Voorhis, T. *J. Chem. Theory Comput.* **2011**, *7*, 594–601.

(92) Bell, T. D. M.; Ghiggino, K. P.; Jolliffe, K. A.; Ranasinghe, M. G.; Langford, S. J.; Shephard, M. J.; Paddon-Row, M. N. *J. Phys. Chem. A* **2002**, *106*, 10089–10088.

(93) El-Khouly, M. E.; Ju, D. K.; Kay, K.-Y.; D'Souza, F.; Fukuzumi, S. *Chem.—Eur. J.* **2010**, *16*, 6193–6202.

(94) Stowell, M. H. B.; Phillips, T. M.; Rees, D. C.; Soltis, S. M.; Abresch, E.; Feher, G. *Science* **1997**, *276*, 812–816.

(95) Sundström, V.; Pullerits, T.; van Grondelle, R. *J. Phys. Chem. B* **1999**, *103*, 2327–2346.

(96) Stockburger, J. T.; Mak, C. H. *J. Chem. Phys.* **1996**, *105*, 8126–8135.

(97) Makri, N. *Annu. Rev. Phys. Chem.* **1999**, *50*, 167–191.

(98) Song, X.; Wang, H.; Van Voorhis, T. *J. Chem. Phys.* **2008**, *129*, 144502.